

MeerKAT@5: New gravity tests with the Double Pulsar in the era of MeerKAT

Huanchen Hu and the MeerTime Collaboration
Max Planck Institute for Radio Astronomy, Germany



MAX-PLANCK-GESELLSCHAFT

Abstract

The MeerKAT telescope opens a new era of high precision pulsar timing in the Southern sky. This brings the accuracy of gravity tests with the Double Pulsar J0737-3039A/B to an unprecedented level and enables precision tests of next-to-leading order (NLO) effects in the orbital motion and signal propagation. Here we present the latest timing results of PSR J0737-3039A based on MeerKAT observations, including the best test of the NLO signal propagation effects that are not accessible in any other pulsar systems, namely the retardation effect due to the movement of pulsar B and the deflection of the signal of A by the gravitational field of B. With only 3 years of MeerKAT data, we obtained improved measurements on the Shapiro delay and NLO signal propagation effects. Moreover, ongoing observations with MeerKAT and the forthcoming SKA are expected to enable new gravity tests as well as provide one of the first measurements of the moment of inertia of a neutron star, thus providing important complementary constraints on the equation of state at supranuclear densities.



Best test of NLO signal propagation effects

The Double Pulsar PSR J0737-3039A/B is the only known system that comprises two pulsars, a 23-ms recycled pulsar A and a 2.8-s young pulsar B [1,2]. These two pulsars reside in a nearly edge-on and slightly eccentric 2.45-hr orbit, offering a rich laboratory for strong-field gravity tests [3]. Comparing with other gravity experiments (including the Event Horizon Telescope), the Shapiro delay measured in the double pulsar probes the strongest spacetime curvature in a precision experiment with photons [4]. MeerKAT observations on PSR J0737-3039A provide extraordinary timing precision, allowing a quick improvement on the measurements of Shapiro delay and next-to-leading order (NLO) signal propagation effects (see Tab. 1) [5].

Logarithmic Shapiro shape, z_s	9.669(77)
Range of Shapiro delay, r (μs)	6.163(16)
NLO factor for signal prop., q_{NLO}	0.999(79)
<i>Derived parameters</i>	
$s \equiv \sin i = 1 - e^{-z_s}$	0.9999369(+46/-51)
Orbital inclination, i (deg)	89.36(3) or 90.64(3)
Mass of pulsar A, m_A (M_\odot)	1.338 186(10)
Mass of pulsar B, m_B (M_\odot)	1.248 866(7)
Total mass, M (M_\odot)	2.587 052(11)

Tab. 1 Shapiro delay parameters and derived parameters of PSR J0737-3039A based on MeerKAT data.

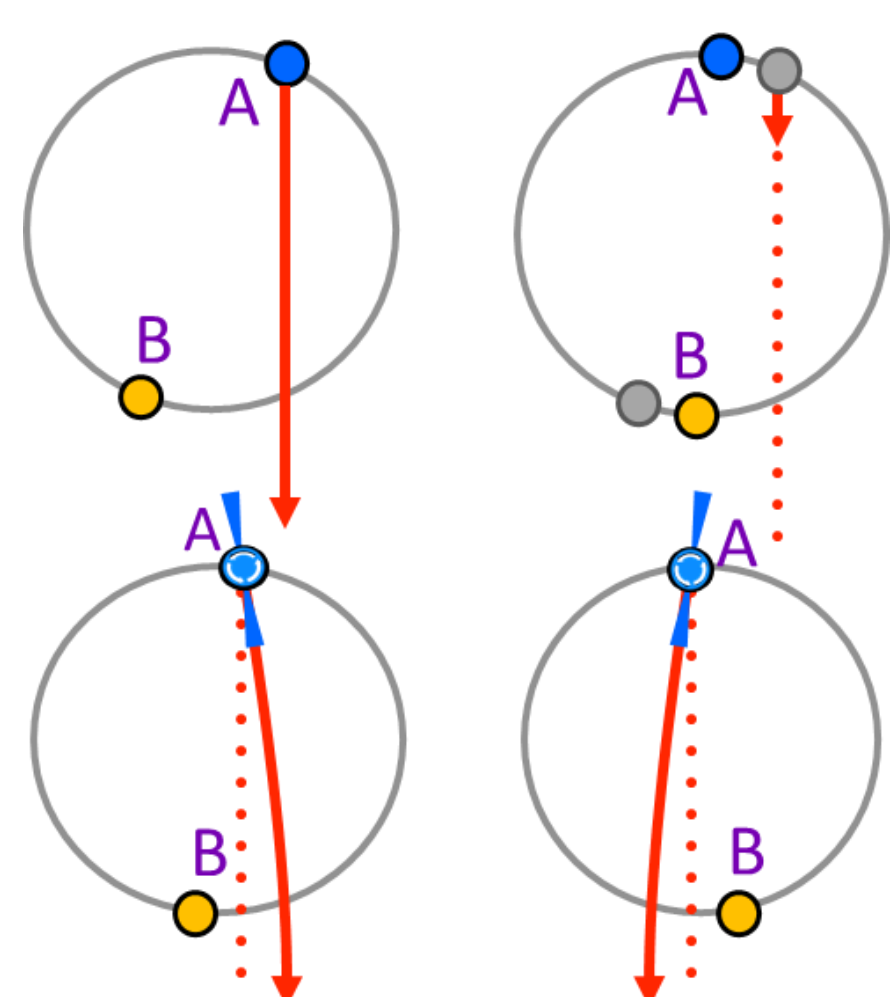


Fig. 1 Top: Retardation effect occurs as pulsar B moves to a new orbital phase while the signal of A propagates across the system. Bottom: Deflection of the signal from the rotating A in the direction of longitude.

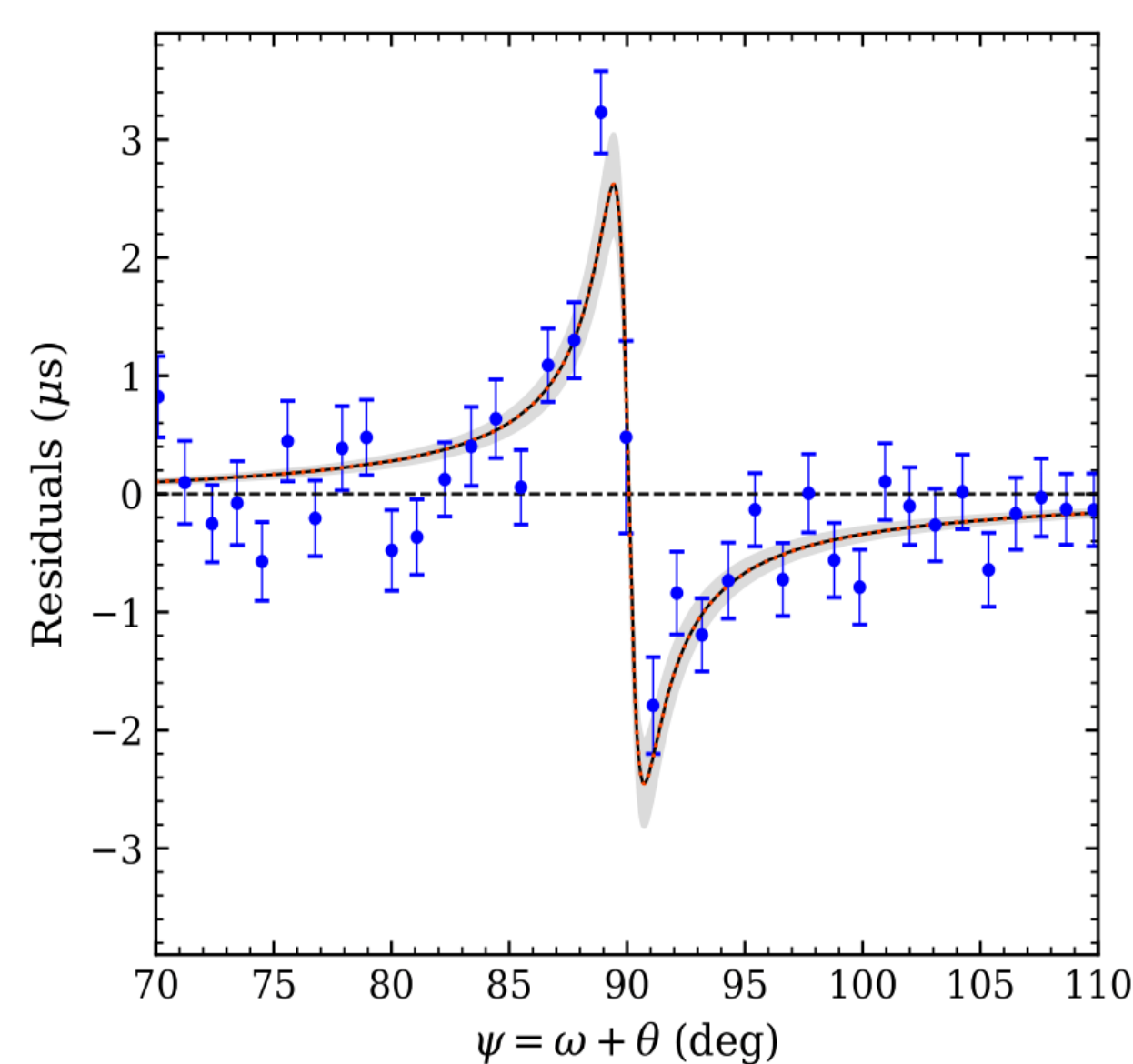


Fig. 2 Residuals showing the combination of retardation effect and longitudinal deflection delay [5].

The NLO signal propagation effects includes the retardation effect due to the movement of pulsar B and the deflection of the signal of pulsar A by the gravitational field of pulsar B, i.e. a lensing correction to aberration (see Fig. 1 for an illustration). With MeerKAT data, the common factor for NLO signal propagation effects ($q_{\text{NLO}}=1$ in GR), including retardation and longitudinal deflection, is measured to be $q_{\text{NLO}}=0.999(79)$, giving an independent confirmation of these effects, which is an improvement of a factor of 1.65 compared to the previous 16-yr result [3], and serves as the best test of these effects.

Latitudinal deflection delay

The lensing correction to the aberration delay may not only lead to a shift in time in the longitudinal aspect but can also result in a change of the co-latitude of the emission direction towards Earth, namely the “latitudinal deflection delay” (see right panel of Fig. 3). This would cause profile variations as the LOS cuts a different region of the pulsar beam.

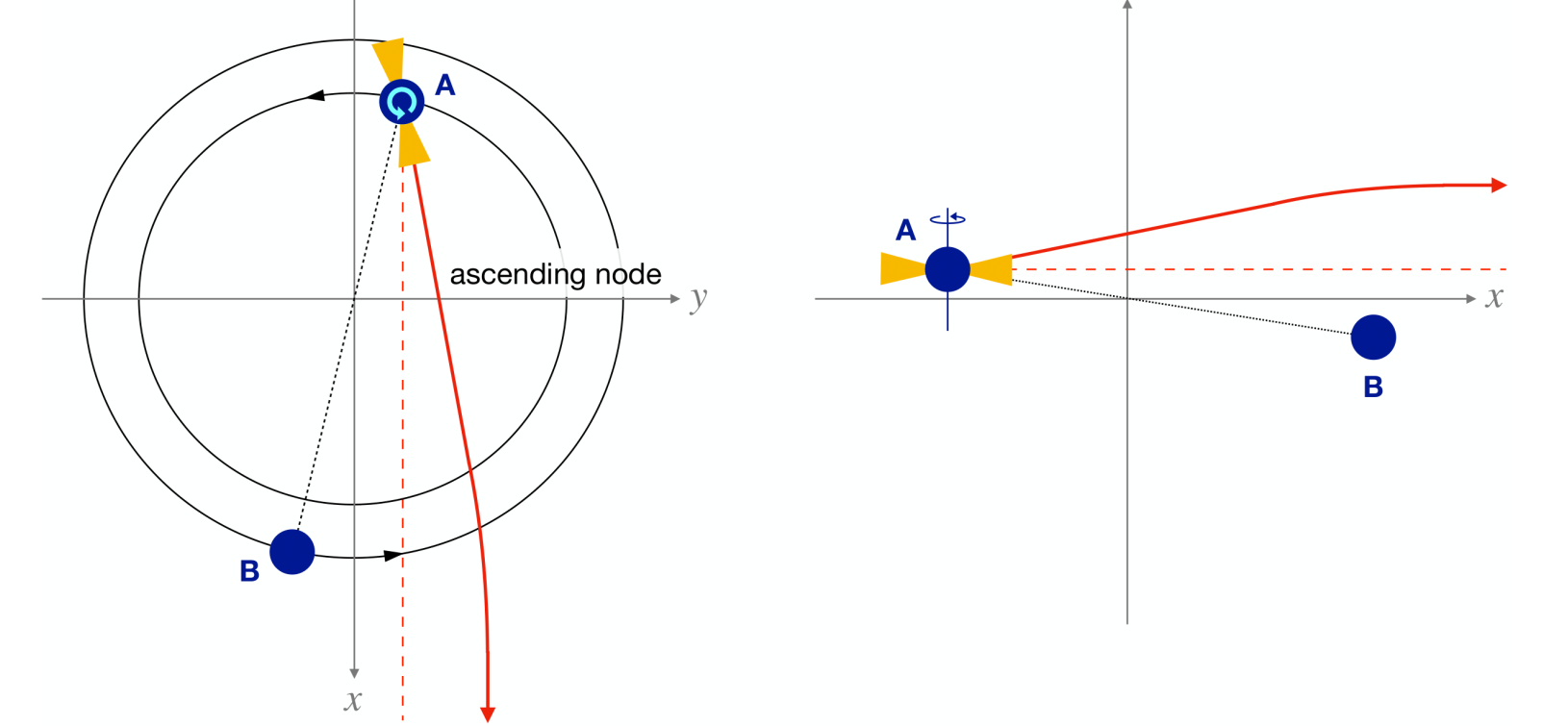


Fig. 3 (left) Illustration of the deflection effect of A's signal in the gravitational field of B, in the direction of longitude (left) and latitude (right) [5].

The profile variation is expected to be maximum at the superior conjunction and symmetric around $\psi = 90^\circ$. We took the eclipse data (an example is shown in Fig. 4, the intensity modulation is caused by the eclipse of the plasma-filled magnetosphere of pulsar B) and added them in orbital phase. We integrated data for orbital phase $89^\circ < \psi < 91^\circ$ with an interval of 0.25° , and compared the profiles with a standard profile. Based on the available data, no significant evidence of profile change was found (see Figs. 8 and 9 in [5]).

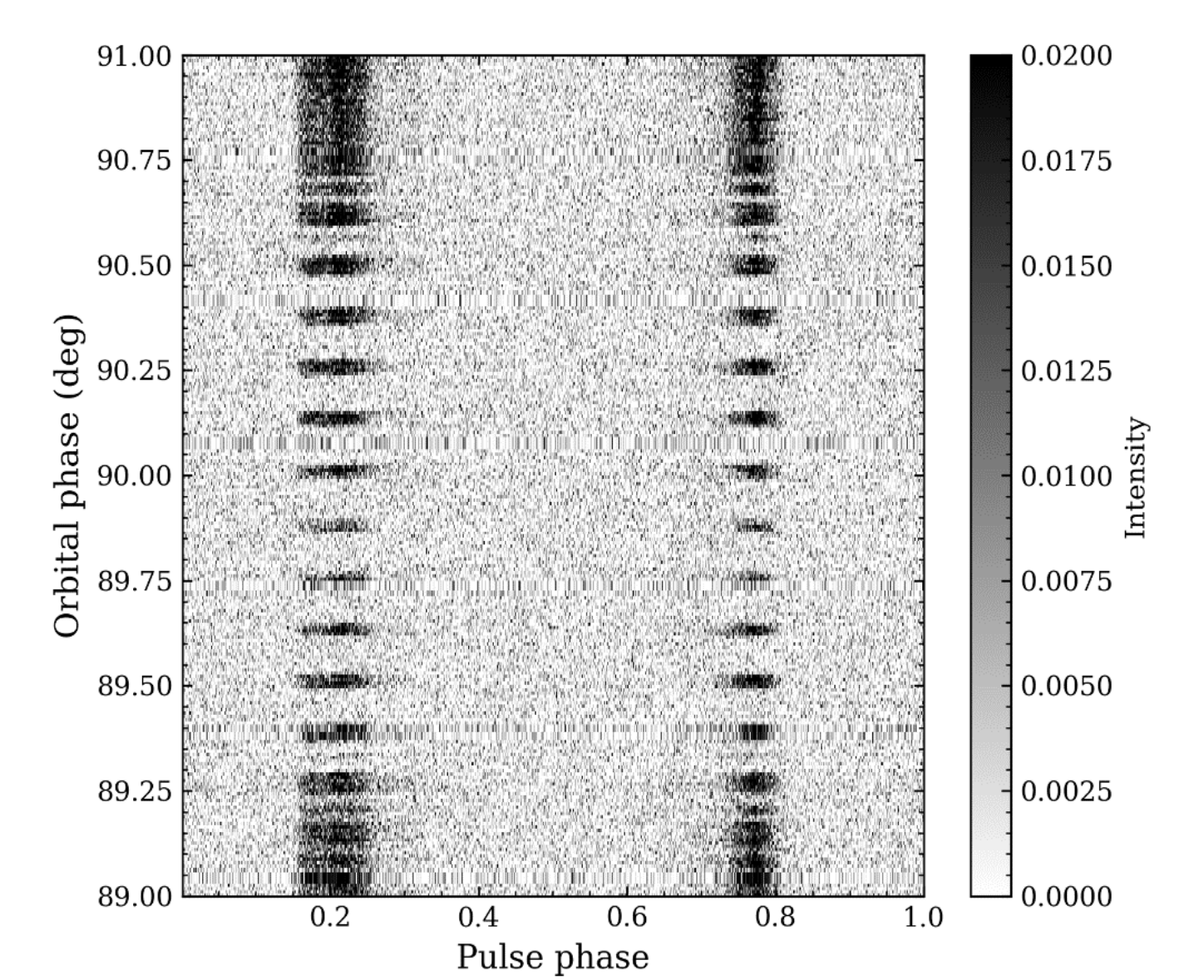


Fig. 4 MeerKAT eclipse data on PSR J0737-3039A.

Lensing correction to Shapiro delay

The leading-order expression of Shapiro delay used in timing model were obtained by integrating along a straight line. We accounted for the lensing correction to Shapiro delay in our model and studied the measurability of this effect. We found this lensing correction is difficult to observe separately as it can be largely absorbed by the Shapiro parameter s , but with the precision of the SKA, it can potentially be measured with a 5- σ precision with ~ 4 years of observation (Fig. 5).

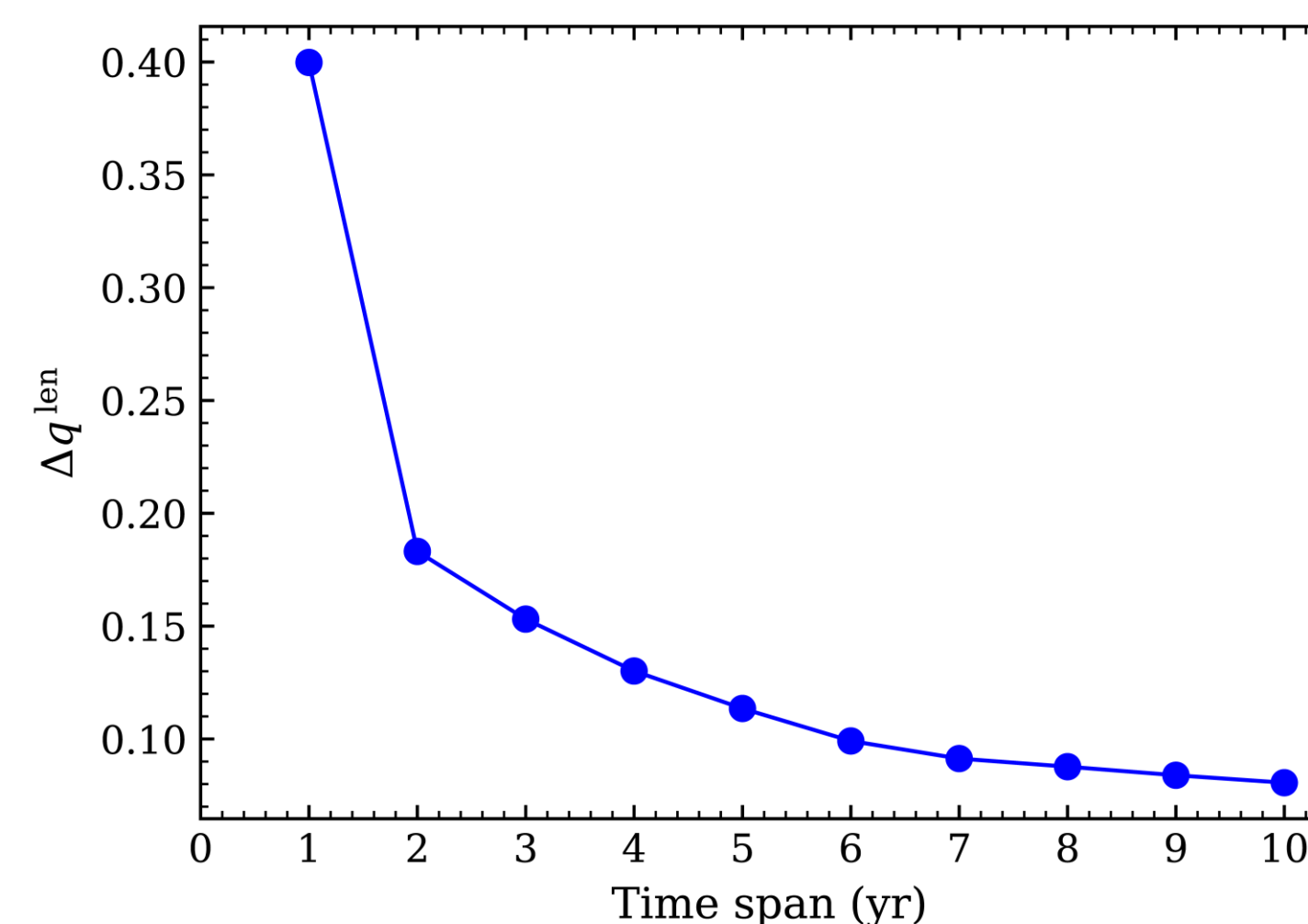


Fig. 5 Uncertainty of the lensing correction factor as a function of timespan for the simulated SKA data.

Moment-of-inertia of a neutron star

Mass measurements from radio pulsars have placed important constraints on the equation of state (EOS) of matter at supranuclear densities. The moment of inertia (MOI) of a neutron star, on the other hand, directly encoding the relationship between mass and radius, can potentially identify the EOS even with a low-precision measurement [6]. For the Double Pulsar, the MOI of A (I_A) will become measurable soon as a contribution to the observed periastron advance due to relativistic spin-orbit coupling (Lense-Thirring effect). With MeerKAT and the SKA, a measurement with $\sim 10\%$ accuracy is possible by 2030 [7], which will provide further constraints on the EOS.

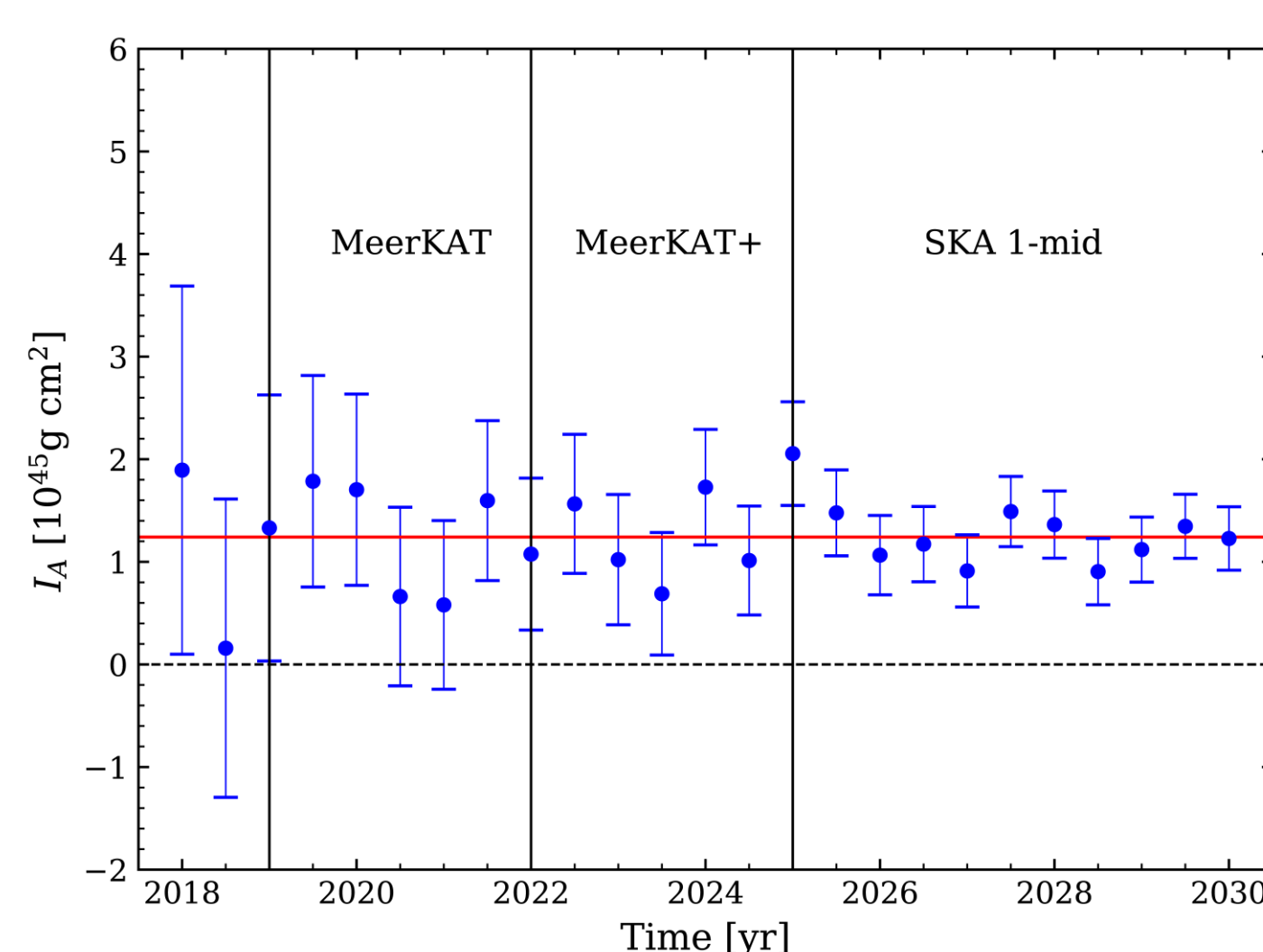


Fig. 6 Simulated measurements of I_A in time with MeerKAT and the SKA.

Testing Lense-Thirring effect

If the EOS is known sufficiently well in the near future, one could in turn test the Lense-Thirring (LT) contribution to the periastron advance in a general form and constrain theories of gravity. It can be written as [9]

$$\dot{\omega}^{\text{LT,A}} = -\frac{2n_b^2 I_A \Omega_A}{(1-e_T^2)^{3/2}} \frac{\sigma_A}{M \mathcal{G}},$$

where σ_A is a generic strong-field spin-orbit coupling constant, and \mathcal{G} the effective gravitational constant (n_b -orbital frequency, Ω_A -angular spin frequency, e_T -time eccentricity, M -total mass). We found a 7% test of LT precession is possible by 2030 [7]. This would be a complementary test to the 13% constraint on σ_B/\mathcal{G} by [8].

NLO gravitational wave damping

In the near future, our data will start to be sensitive to the NLO (3.5PN) GW damping, and a 3 σ -measurement can be expected by 2030. The right side shows the expression of orbital period decay due to GW damping extended to 3.5PN in the equations of motion [10] (see [7] for details).

$$\dot{P}_b^{\text{GR}} = -\frac{192\pi}{5} \frac{\eta \beta_0^5}{(1-e_T^2)^{7/2}} \left\{ 1 + \frac{73}{24} e_T^2 + \frac{37}{96} e_T^4 + \frac{\beta_0^2}{336(1-e_T^2)} \left[1273 + \frac{16495}{2} e_T^2 + \frac{42231}{8} e_T^4 + \frac{3947}{16} e_T^6 - \left(924 + 3381 e_T^2 + \frac{1659}{4} e_T^4 - \frac{259}{4} e_T^6 \right) \eta + \left(3297 e_T^2 + 4221 e_T^4 + \frac{2331}{8} e_T^6 \right) \frac{\delta m}{M} \right] \right\}$$

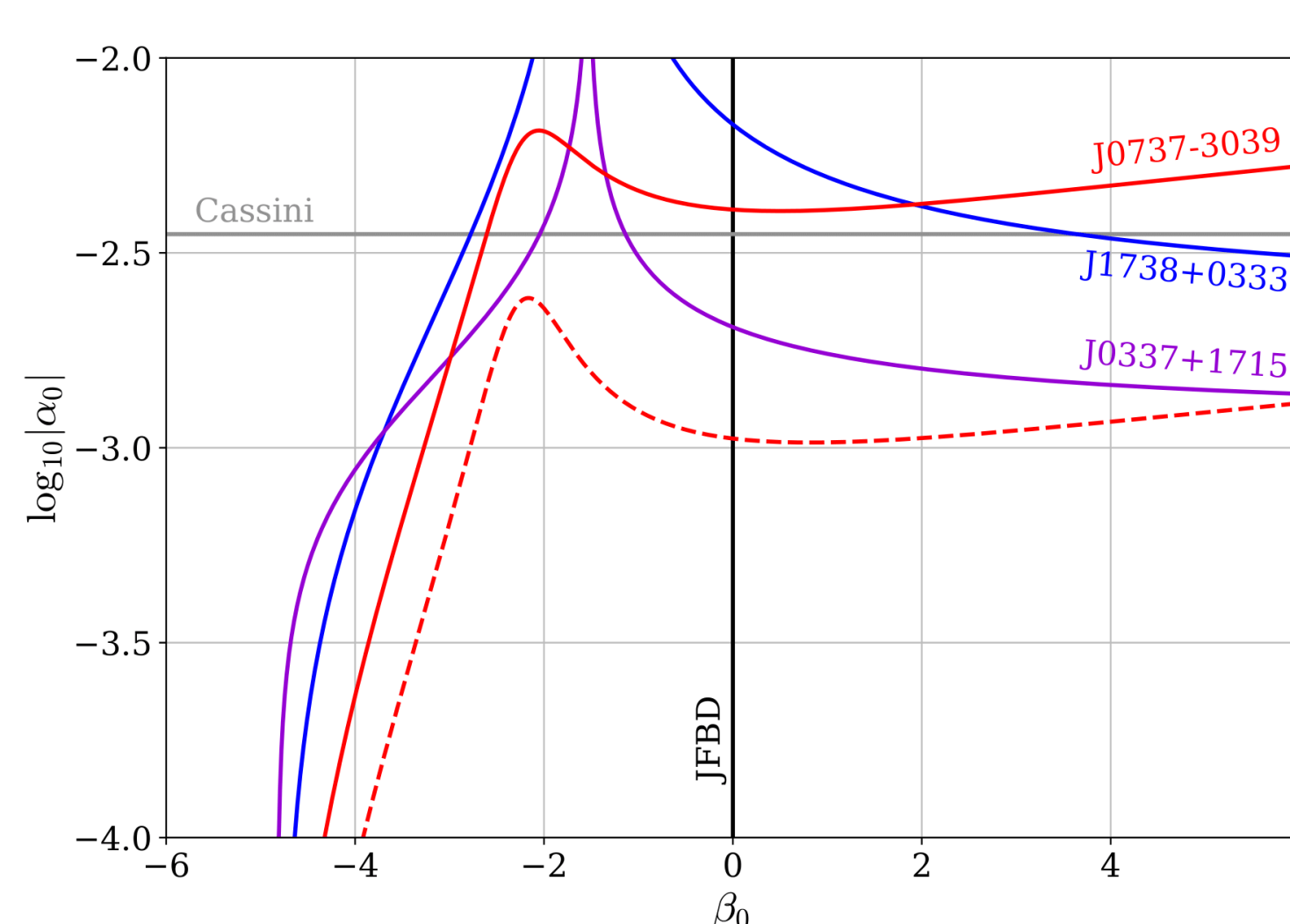


Fig. 7 Constraints on the DEF gravity from different pulsar experiments (see [3][7] for details). A stiff EOS MPA1 is assumed. Areas above a curve are excluded.

Testing alternative theories of gravity

Pulsars also provide constraints on alternative theories of gravity, as dipolar GWs may exist in such theories and could be a leading contribution of GW damping. Fig. 7 summarises constraints on Damour-Esposito-Farèse (DEF) gravity [11] from various pulsar experiments. Despite relatively low asymmetry in their compactness, the Double Pulsar still contributes important constraints for $\beta_0 \lesssim -3$ (red solid line) [3]. With the simulated MeerKAT and the SKA data from [7], we expect an even better constraint from J0737-3039 by 2030 (red dashed line).

References

- [1] Burgay et al., 2003, Nature, 426, 531
 [2] Lyne et al., 2004, Science, 303, 1153
 [3] Kramer et al., 2021, PRX 11, 041050
 [4] Wex & Kramer, 2020, Universe, 6(9), p. 156
 [5] Hu et al., 2022, A&A, 667, A149
 [6] Lattimer & Schutz, 2005, ApJ, 629:979
 [7] Hu et al., 2020, MNRAS, 497, 3, pp.3118-3130
 [8] Breton et al., 2008, Science, 321, pp.104
 [9] Damour & Taylor, 1992, PRD, 45, 1840
 [10] Blanchet & Schäfer, 1989, MNRAS, 239, 845
 [11] Damour & Esposito-Farèse, 1993, PRL, 70, 2220